Graphene-Like Layers from Unconventional Carbon Sources: New Perspectives on Hybrid Materials and π-system Synergisms

Roberto Di Capua[1*], Valentina Gargiulo[2], Michela Alfè[2]

[1]Department of Physics - University of Naples Federico II, and CNR-SPIN, I-80126 Naples, Italy
[2]Istituto di Ricerche sulla Combustione (IRC) - CNR, I-80125 Naples, Italy

Article info	Abstract
	We developed a new approach for producing graphene-like (GL) materials through a two-steps oxidation/reduction method starting from a nanostructured (high surface) carbon black, a versatile carbonaceous material prone to be structurally and chemically modified in quite mild wet conditions. Atomic Force Microscopy and zeta-potential measurements allowed to model the assembling mechanisms and the role of hydrophobic interactions, demonstrating the possibility to easily tune the surface morphology. GL materials have been then employed in a large variety of hybrid materials for innovative applications, and characterized by chemical, electrical, structural and spectroscopic techniques. With Metal-Organic Frameworks, GL produced conducting composites with electrical conductivity tunable by changing the concentration of the parent materials; Eumelanin/GL and TiO_2-nanoparticles/GL were also studied for photocatalysis and biosensors applications.

1. Introduction

The term graphene refers to a single-layer graphite with peculiar physical, chemical, and mechanical properties [1–8]. Graphene is largely employed for the fabrication of electronic devices, and it is considered a promising candidate for optoelectronic devices. The usage of graphene is now covering several fields of application: graphene-based window electrodes can be used in the production of solid-state dye sensitized solar cells [9] and of light-emitting diode (LED), as well as in liquid crystal technologies [10]; graphene is also involved in the fabrication of energy-storage materials [11] and mechanical resonators [12]; it can be used as channel material for the next generation of field emission transistors (FET), or as conductive sheet upon which nanometer scale devices may be patterned to create single- or few electron transistors [13]; graphene is also used as nanofiller in the production of polymeric nanocomposites with improved functional features [14].

Besides the isolated, single-atom-thick carbon sheets (universally referred to as graphene), related two-dimensional sheet-like or flake-like carbon forms, possibly exhibiting different surface functionalities, are gaining increasing interest for fundamental and applied research. As a consequence, a large number of graphene-related systems are now studied: ultrathin multilayer materials produced by graphite exfoliation are already of significant commercial interest as composite fillers; few-layer materials with either ABA stacking or rotational faulting giving rise to electronic decoupling of the individual layers [15]; other chemically modified graphenes (the simplest one being the graphene oxide) [16], or different carbon materials realized using graphene or graphene oxide as atomically-thin precursors, can be used to build a large number of three-dimensional (3D) architectures [17, 18]. Together with monolayer graphene, these systems constitute a family of ultrathin, two-dimensional carbon materials, most of which are new, and with established or potential scientific and technological interest. In addition to the specific aggregation form of carbon layers, surface functional groups (in particular the oxygen-based ones) are also recognized to play a great role in many possible applications of carbon materials [19–24]. For example, the acidic surface functional groups constitute the main factor governing the dynamic adsorption of hexane by activated carbons under humid conditions [25];

---

*Corresponding author. E-mail: rdicapua@na.infn.it

oxygen surface complexes, possibly lactone and carbonyl groups, have been found to be the active sites for Hg-0 capture [26]; microorganism fixing is enhanced by the increase in the number of some acid functional groups and by the surface wetting quality [27].

Another remarkable research field involving graphene and graphene related materials is the realization of composites and heterostructures [28]. The presence of oxygen-containing functional groups as a consequence of different synthesis processes from several precursors, makes possible the tuning of graphene derivatives properties. Such a powerful possibility allows to employ graphene derivatives in conjunction with a large class of materials to build composites with different features. As a consequence, incorporation of graphene-like materials has been realized in organic and inorganic crystals or nanostructures [29–33], polymers [14, 34], biomaterials [35–37], carbon nanotubes [38–42], metal-organic frameworks [43–45].

At the present, the bottleneck for the development of a large scale graphene-based technology is its production on a large scale. Several approaches have been reported for the production of graphene or graphene-like materials: one-step graphite exfoliation [46], chemical vapor deposition (CVD) of methane gas [47], graphite stamping [48], graphite oxide reduction [49], and carbon nanotube unzipping [50]. Among the reported fabrication methods, the production of graphite oxide (GO) from graphite powder and its further reduction (through chemical [49–51], thermal [52, 53], or ultraviolet-assisted reduction [54] methods) to graphenic material is considered a convenient and economic way for the fabrication of graphene sheets.

Here, we illustrate a method to produce graphene-like (GL) layers starting from water suspension of oxidized carbon black (CB), through a two-steps oxidation/reduction process. CB is mainly constituted of hydrophobic material organized, at nanoscale level, in graphene layers with various degree of deviation from planarity [55, 56], with a certain amount of less organized areas (amorphous and disordered carbons) that makes CB particles more reactive than graphite. We report basic and advanced characterization of the synthesized samples, to infer their main chemical, physical structural and morphological properties. In particular, we studied the effect of pH of the starting suspension on the morphology of self-assembled GL films, showing how it is possible to tune it and how such behavior can be effectively interpreted from a microscopic point of view. As an example of potential technological application of our GL layers, we describe

their incorporation in MOFs matrices and the resulting properties; we also mention the first studies concerning the realization of composites with TiO_2 nanoparticles and of hybrid structures with eumelanin pigments, in view of applications in catalysis and biosensors technology respectively.

2. Experimental and Discussion

CB was purchased from Phillips Petroleum Co. and classified as N110 (corresponding to aggregates of rounded primary particles with a diameter of 10–15 nm) carbon black (furnace carbon black), according to ASTM classification. Its density at 25 °C is 1.8 g/mL and the specific BET area is 151 m^2/g.

Transmission electron microscopy shows that CB is arranged in chainlike aggregates of spherical primary particles [57]. The particle average diameter is 15–20 nm, with a narrow size distribution. The nanoscale organization of carbon black primary particles is typical of a disordered carbon. More organized regions are observed with a concentric organization of the stacked graphitic layers extending throughout each primary particle. H/C atomic ratio is 0.058 and the temperature of the maximum combustion rate is 690 °C. The hydrodynamic diameter of each CB aggregate is narrow (180 ± 20 nm) as confirmed by dynamic light scattering (DLS) performed on CB suspension in N-methylpyrrolidinone (NMP), a solvent very effective for the coal extraction [58].

The oxidation step follows the procedure reported by Kamegawa et al. [59]. 500 mg of CB powder was treated with 10 mL of nitric acid (67% wt.) at 100 °C under stirring for 90 h. After cooling at room temperature, the aqueous suspension was centrifuged (at 3500 rpm for 30 min) obtaining an acid-soluble fraction (AS) and an acid-insoluble fraction (AI). The AS fraction, containing mostly unreacted acid and hexacarboxylic acid (mellitic acid), was discarded. The AI was washed with distilled water (100 mL) and recovered after centrifugation (3000 rpm, 30 min). This purification step was repeated until acid traces were successfully removed. The product had a dark brown appearance and it was not as opaque black as the pristine CB. The hydrophilic product was dried at atmospheric pressure at 100 °C and labeled as GLox.

The reduction of GLox was performed by applying the procedure with hydrazine hydrate proposed for GO by Stankovich et al. [49]. In GO treatment, the reduction is an essential step in order to transform it back into a conductive graphitic material as a consequence of the partial restoration of the graphitic structure. The solution route through chem-

ical reduction with hydrazine is the more advantageous one because a large amount of GO in the solution phase can be easily converted to graphene-like nanosheets through the partial removal of oxygenated functional groups present in the structure of GO [60, 61]. We adopted a similar procedure for GLox. The GLox powder (20 mg) was suspended in 20 mL of distilled water in a 50 mL round-bottom flask yielding a homogeneous dark brown dispersion. The dispersion was treated with 450 µL of hydrazine hydrate (50%). The dispersion was heated in an oil bath at 100 °C under reflux for 24 h applying a constant stirring. At the end of the reaction the excess of hydrazine was neutralized with nitric acid (4 M) and the resulting black solid recovered by centrifugation (3000 rpm, 30 min). To remove traces of reagents and acid, the solid was washed with distilled water and recovered by centrifugation three times. The product was dried at atmospheric pressure at 100 °C and labeled as GL. The dried GL was insoluble in water and in the most common organic solvents, both polar and apolar (water, ethanol, NMP, dichloromethane, heptane, dimetilformammide). This was attributed to an increase in hydrophobicity of the material caused by a decrease in the polar functionalities on the surface and consequent intimate self-assembling interaction between the restored graphitic planes. For this reason the preparation of the film for investigation by atomic force microscope (AFM) was performed allowing a drop of the GL water suspension drying directly on the mica plate.

An advantage of the adopted selected oxidative treatment, is that it provides the partial demolition of the CB microstructure and the functionalization at the edge of the basal planes of the graphitic layers [62], and not on them. Inside water suspension, GL layers are made by small flat nanoparticles decorated at the edge with oxygen functional groups (mainly carboxylic/carbonylic and hydrazones), and the graphenic basal planes are untouched [63]. Therefore, differently from what happens for GO, the original graphitic network is preserved in the oxidized CB, which represents a clear advantage for the conductivity and the electronic properties. In addition, this method allows scalability and potentially large-amount production of GL layers at reduced costs.

The effects of the reduction process on the synthesized films have been investigated also by Raman spectroscopy and UV–visible spectroscopy, whose main results are reported elsewhere [63]. Briefly, the features of the Raman spectra are consistent with the occurrence of a multilayer structure. D ad G bands have, in the spectra, compa-rable heights, indicating a significant structural disorder. We also found that the reduced GL layers and the unreduced ones have very close values for the D-band to the G-band ratio, a clear indication that the oxidation process preserves the presence of the graphitic network, and that the chemical functionalization occurs at the edge and not at the basal planes of the GL layers. The preservation of the graphitic network in the reduction process is confirmed by UV–visible spectroscopy; furthermore, the collected spectra on GL layers are blue-shifted compared to the ones on CB, indicating a decrease in the size of the π conjugation domains. H/C atomic ratios changed from 0.058 in raw CB, to 0.27 and 0.32 in GLox and GL respectively. Electrical dc-measurements, realized in a standard four-contact van der Pauw geometry, revealed that reduced samples (GL layers) exhibit quite good conducting behavior, their resistivity being of the order of 1 $\Omega \cdot m$. Such conducting properties can be exploited, for example, for the incorporation in insulating matrices to enhance their conducting properties. A sketch of the two-step method is reported in Fig. 1.
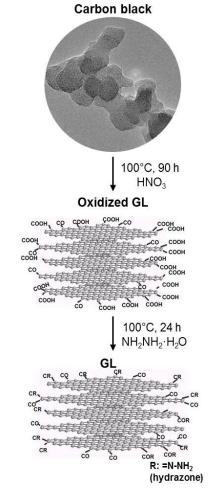

Fig. 1. Sketch of the two-step method for the preparation of GL layers from CB.

The pH of the as-prepared GL layers water suspension was 3.70. We studied the effect of pH variation on the morphology and on assembling properties of GL films.

An investigation of residual functional groups on the surface of GL, and of its acid-base behavior, was performed by coulometric–potentiometric titration for 2.7 < pH < 7 (into an air thermostat at the temperature of 25 °C), in NaCl 0.25 M, measuring the potential of a glass electrode sensitive to proton activity. The current intensity was accurately determined by reading the potential drop at the ends of a calibrated resistance coil, connected in series to the coulometric device. We identified two functional groups on the surface in the carboxylate region (pK 2.0–5.0) [64], having $pK_a = 3.40 \pm 0.05$ (number of sites: 900 ± 30 mmol/g) and $pK_a = 5.5 \pm 0.1$ (number of sites: 240 ± 30 mmol/g) respectively. The higher pK_a value (5.5) is ascribable to the presence of lactones and carboxylic anhydride groups that tend to hydrolyze in the presence of acids and bases [65]. More technical details can be found in [66]. The presence of residual carboxylic groups is also confirmed by X-ray Photoemission Spectroscopy (XPS) performed on the GL surface [66].

The stability of the GL layers water suspensions was evaluated by zeta potential analyses. Figure 2 shows the measured zeta potentials as a function of pH of the suspension. The zeta potential value of the GL dispersion was negative in all the range of investigated pH, indicating the presence of partly preserved anionic charge. Its dependence on pH value can be interpreted in terms of ionization of residuals of carboxylic groups: such ionization is indeed responsible of the anionic charge, and it is strongly related to pH. Zeta potential values lower than –30 mV are conventionally considered as an indication of sufficient mutual repulsion to ensure
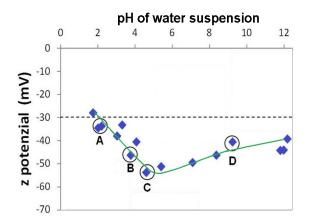
the stability of dispersions [67]. By adopting this criterion, we concluded that GL dispersion was stable in a wide range of pH values: zeta potential was below –30 mV for pH greater than 2, and it reached –45 mV when the pH approached 12, with a minimum of about –55 mV for pH between 4 and 5.

For a deeper investigation we selected four pH values, particularly meaningful: 2.0, 3.7, 4.6 and 9.5, which in the following are indicated as Sample A, B, C, D, respectively. Sample A (pH = 2.0) corresponds to GL layers in acid suspension at the limit of the stability range of the suspension (zeta potential very close to –30 mV); Sample B (pH = 3.7) represents "as prepared" GL layers suspension; Sample C (pH = 4.6) is obtained from the GL layers suspension on which the minimum zeta potential was recorded; Sample D (pH = 9.5) is a representative of GL layers in basic suspension.

Mica plates, atomically flat, were used as substrates for AFM morphology measurements to infer information about the surface quality of the films after drying. Each GL layers water dispersion at the selected pH points, at the concentration of 1 mg/mL, was drop-casted onto freshly cleaved mica substrates and dried at room temperature.

The topographic images acquired on the four investigated samples are reported in Fig. 3. All the shown images are recorded on a 5 μm × 5 μm area, acquired in the True Non ContactTM mode of operation of the XE-100 Park system. Line profiles, indicative of the surface morphologies, are also reported.

The surface of Sample A (Fig. 3 a), prepared in acid suspension at the limit of the stability range, appears very rough, and characterized by grains having width of the order of one or few hundreds nanometers. The resulting peak-to-peak roughness of the surface is about 50–100 nanometers.

The granular appearance of the surface of Sample A is extremely different from the morphology measured on the other three samples prepared in suspensions with higher pH.

Both Sample B and Sample C exhibit atomically flat surface over large areas (Fig. 3 b and c). On the surface of Sample C, however, there are some isolated "islands" having different lateral sizes. A comparison of statistical roughness from these samples with sample A reveals than on Sample A the grains lead to a root mean square roughness of about 43 nm, while on the collected image on Sample B it is less than 1 Å and on sample C it is about 9 Å. We selected a line profile crossing the largest island on the surface of Sample C; the profile shows steps of vertical height slightly more than 4 nm, and terraces characterized by the same flatness
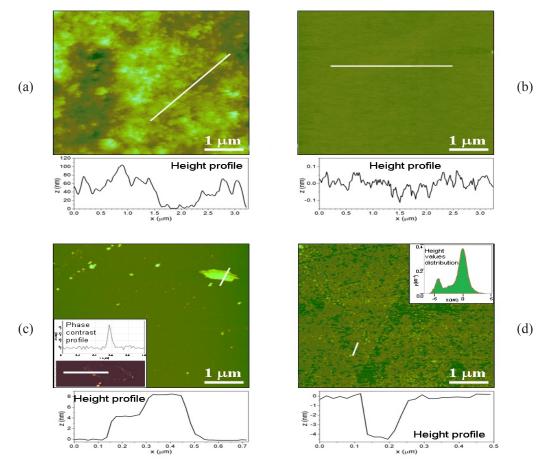

Fig. 2. Zeta-potential of the GL layer suspensions (0.05 mg/mL) as a function of the pH of the suspension itself. (adapted from [66]).

Fig. 3. 5 μm × 5 μm AFM images on the four investigated GL samples, together with line profiles: a) Sample A; b) Sample B; c) Sample C (in the inset, the phase contrast profile on a line crossing the large "island" on the top-right of the image); d) Sample D (in the inset: histogram of the distribution of measured height values on the image). (adapted from [66]).

of the surrounding surface. Such flatness suggests that the observed islands and the surrounding carbon surface are actually made by the same material, and seems to exclude that the island are constituted by spurious phases or unrelated particles. The phase contrast image confirms this conclusion: the phase image in the noncontact AFM scan (repulsive van der Waals regime, amplitude modulated oscillation) is indeed able to provide qualitative information about the chemical nature of the imaged surface, the phase shift of the induced oscillation being sensitive to the chemical functionalities of the surface itself (through differences in the mechanical interaction between the tip and the surface itself). The inset in Fig. 3c shows a phase profile taken across the edge of the island, showing that non significant phase shift is detected between the main surface and the island: it has been shown on graphene nanosheets produced by chemical reduction of graphene oxide [68] that the different degree of hydrophilicity and hydrophobicicity or differently oxidized regions are revealed by a phase upper-shift of the order of 2°–3°, which are well

above the sensitivity of our instrument, as can be seen in the inset of Fig. 3c.

Sample D, representative of samples obtained in basic suspension, shows an "uncompleted" layer over an underlying flat surface: the topographic image (Fig. 3d) exhibits regions with lacks in the topmost surface. The histogram (in the inset of Fig. 3d) of the measured relative heights forms a clearly bimodal distribution, confirming this circumstance. The peak of the histogram at the higher height value is associated to the upmost layer, while the presence of the second peak at a lower height value indicates that all the "holes" in this layer have basically the same depth. Interestingly, from the peak separation of the histogram as well as from the reported topographic profile, it can be seen that the vertical separation between these two layers is between 4 and 5 nm. The same value or doubled is measured on the isolated "brighter" spot on the surfaces, also resembling what already described for the surface of Sample C. These observations suggest that the uncompleted layers of Sample D, as well as the large island imaged on the surface of Sample C, could be

seeds for further layers. Surprisingly, these layers seem to have a "fundamental" vertical thickness of more than 4 nm: in Ref. [63], AFM scans on our fractured flat GL samples seemed to show steps having the same basic vertical unit.

The dependence of the morphological features of the GL samples on the pH of the water solution can be interpreted in terms of forces acting into the water suspension and the resulting aggregation processes between GL particles. The increase of the pH of the solution corresponds to an increase of the charge density due to the progressive deprotonation of the residual carboxylic functional groups (the carboxylic groups are progressively converted in the anionic form $-COO^-$). The GL layers acquire therefore a more hydrophilic character going from Sample A to Sample D, monotonically. A greater hydrophilicity makes the formation of GL–water interfaces energetically more favorable, leading to a positive spreading coefficient [68] and to the consequent formation of "wet" GL layers. Differently speaking, the energetically favorable interface formation corresponds to a low surface tension between GL layers and water, and to the consequent tendency to maximize the contact surface. This is the situation occurring in Samples B, C, D, for which flat layers are formed in the solution. On the contrary, in Sample A, grown in a suspension with lower pH, the surface charge tends to decrease as a consequence of the presence of the carboxylic groups at the edge of the GL layers in the neutral form (COOH). The result is that GL layers are forced to aggregate to minimize the contact with the polar solvent, producing the grains observed in the AFM image. An interpretation of the crossover between the two regimes in terms of microscopic forces between elementary constituents, i.e. in terms of competition between van der Waals (vdW) and electrostatic double layer (DL) forces, is reported in ref. [66].

One potential application of our GL films that we explored was their incorporation inside metal-organic frameworks (MOFs) [70]. MOFs are obtained by the assembly of metallic centers and organic linkers in a coordination network, through strong covalent bonds. They are characterized by high crystallinity and uniform porosity. MOFs attracted a strong interest in the last years, because of their high surface area (up to 4500 m^2 g^{-1}) [71] and the possibility to tune their chemico-physical and textural properties by varying their metallic centers and organic functionalities [72], that makes them suitable for a large array of specific applications. For the large internal surface area and high porosity and crystallinity, MOFs are often compared to zeo-

lites. Similarly to zeolites, MOF have been utilized in some applications including adsorption and separation of specific gases [73], gas storage [74–78], heterogeneous catalysis [79] drug delivery [80] and chemical sensors [81]. Compared to zeolites and other porous inorganic solids, however, MOFs have some disadvantages, such as the tendency of reversible binding of water, the air- and moisture sensitivity and a lower chemical and thermal stability [71]. In addition, MOFs exhibit an electrically insulating character, which made their transport properties rarely studied. In order to overcome the weak points of MOFs and to expand their field of applications, it has been proposed the preparation of composites involving MOFs and carbon-based materials (including carbon nanotubes [82], graphite oxide [45], graphite [83]), in which the properties of carbonaceous surfaces and MOFs are combined. Studies on MOF-5 (a zinc-based MOF), for example, show that its intercalation with graphene decorated at the basal plane with carboxylic groups exhibits new electrical properties [43]. The introduction of carbonaceous material into MOF structure can lead to an enhancement in non-specific adsorption improving the kinetics of adsorption. Furthermore, the conductivity and the high specific surface area of graphene can positively affect the dielectric and conducting properties of host materials, which could fulfill the recently highlighted request for MOFs with conducting properties for several applicative purposes [43, 84].

Following this ideas, we incorporated our conductive GL layers in a copper-based MOF, containing Cu^{2+} dimers as the metallic units linked to oxygen atoms from benzene tricarboxylate (BTC) [85–86], and referred in literature as HKUST-1 or MOF-199. HKUST-1 combines high surface area, water stability [87], simple preparation procedure (anhydrous conditions are not required) at low costs conditions (since precursors are easily available and not expensive). We prepared and characterized HKUST-1 samples and MOF/GL composites (MGL) as described in [70]. Four MGL composites were prepared, indicated as MGL-1, MGL-2, MGL-3, MGL-4 in the following, having different GL percentages: 5, 15, 30, 40% wt., respectively. For all the produced composites, the liquid phase recovered after the filtration of the crystals resulted colorless, indicating a complete incorporation of the GL material into the MOF structure, and the percentage of the incorporated GL was checked by elemental analysis and inductively coupled plasma mass spectrometry [70]. The elemental composition of all the investigated samples of this comparative study is reported in Table 1. Table 1 also

Table 1
Elemental composition, BET area and pore volume of MGL composites and parent compounds.

Sample	GL content (wt.%)	Elemental composition (wt.%)					BET area (m^2g^{-1})	Pore volume (cm^3g^{-1})
		C	O	H	Cu	N		
HKUST-1	0	26.64	34.69	2.45	35.7	0.52	1989	0.98
MGL-1	5	29.64	31.19	2.47	35.5	1.20	906	0.74
MGL-2	15	32.07	29.05	2.01	35.1	1.77	709	0.67
MGL-3	30	38.33	32.51	2.03	24.4	2.73	582	0.62
MGL-4	40	39.22	33.38	1.65	22.7	3.05	570	0.45
GL	100	52.60	39.61	1.40	0	6.09	76	-

reports the BET specific surface area and pore size distribution of the samples (Ar adsorption at 87 K). The measured BET surface area on HKUST-1 is comparable to the values reported in the scientific literature [45,71] whereas pure GL exhibits a much lower surface area. In the composites, both surface area and pore volume decrease, compared to HKUST-1, with the progressive incorporation of GL. The first incorporation of GL into HKUST-1 in a low amount (5% wt.) produces a dramatic reduction of surface area. On the other hand, further incorporation of GL causes smaller reduction of the surface area, roughly proportional to the fraction of GL. These occurrences indicate that a small fraction of GL is sufficient to modify the HKUST-1 structure, creating a new kind of porosity at the interface between the GL and MOF components.

Figure 4a shows the ATR-IR spectra of the parent materials (HKUST-1 and both GLox and GL) and of the MGL composites, in the 2000–700 cm^{-1} wavenumber range. Spectra are baseline corrected and shifted for clarity. The highly conjugated p-network of GLox and GL caused peak broadening in their ATR-IR spectra due to the overlapping of several vibrations in the 1000–1500 cm^{-1} range [88]. Both spectra exhibit bands at 1750–1650 cm^{-1} (ascribable to C=O stretching vibrations from carbonyl and carboxylic groups) and 1600–1500 cm^{-1} (skeletal vibration of the sp^2 graphitic domains). In the GLox spectrum, an enhanced broad band in the 1300–1100 cm^{-1} region is observed, ascribable to the overlapping of C–OH and C–O stretching vibrations. The intensities of the C=O band and of the broad band are significantly weaker in the GL as a consequence of the partial removal of carboxylic–carbonylic functionalities upon the reductive treatment. In the ATR-IR spectrum on HKUST-1, the bands at 1645 and 1590 cm^{-1} and at 1450 and 1370 cm^{-1} correspond to the asymmetric and symmetric stretching vibrations of the carboxylate groups in BTC, respectively [45, 89]. The features in the

ATR-IR spectra of the composites are similar to those observed on HKUST-1: a remarkable difference, however, is the absence of the C=O bands in the composites ATR-IR spectra. This circumstance suggests that the carboxylic functionalities of the GL interacts with the copper dimers, and chemical interactions are involved in the formation of the composites. It can be speculated that the presence of residual carboxylic groups, located at the edges of the graphenic basal planes, favors the interaction with the MOF crystals, similarly to what observed for MOF/GO composites [45]. Interestingly, the formation of the MOF crystal seems to be not affected, as shown by X-ray diffraction (XRD) investigation [70], by the inclusion of GL. Indeed, Fig. 4b shows that the XRD patterns on composites is similar to the one recorded on HKUST-1, revealing the existence of the well-defined MOF units in the composites themselves. This represents a clear indication that the presence of GL in the reaction mixture does not prevent the formation of linkages between Cu ions and the BTC molecules, leading to the formation of HKUST-1 crystals. Considering the limitations of composite formation addressed in some works [83, 90], this represents a remarkable result.

We performed electrical dc measurements on MGL composites pressed in pellets (evaluating the electrical resistivity according to the van der Pauw method) in order to understand a possible effect or trend due to GL incorporation. The electrical dc conductivity (or resistivity) of HKUST-1 and MGL is a useful macroscopic characteristic for a preliminary comparative analysis of the transport properties, since it is governed by both the microstructures and chemical composition.

As expected, the pristine HKUST-1 exhibited a substantially insulating behavior, while on the carbonaceous "counterpart" GL we measured a dc resistivity of about 1.3 $\Omega \cdot m$ (corresponding to a conductivity of 0.77 $S \cdot m^{-1}$). On the composites, we
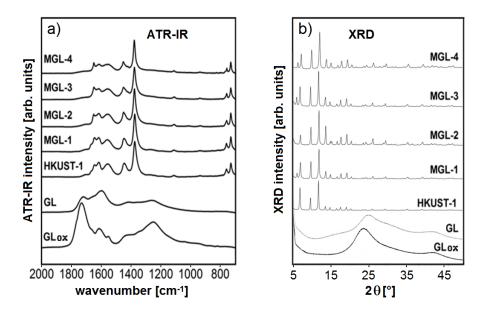
Fig. 4. a) ATR-IR spectra and b) XRD patterns on parent compounds and MGL composites. (adapted from [70]).

found that the electrical conductivity is a rapidly increasing function of the added graphene-like percentage (Fig. 5): changing the GL amount between 5% and 40% wt. makes the electrical dc conductivity increasing of about 5 orders of magnitudes. The increase does not follow a linear behavior: we measured a conductivity of the order of 10^{-7} S·m^{-1} when the graphene-like percentage is 5% wt. or 15% wt., increasing about ten times at 30% wt. of GL content, and becoming 10^{-2} S·m^{-1} when the graphene-like percentage is 40% wt.

Comparable or even larger variations of electrical conductivity were reported also in experiments with CB filling polymeric or epoxy matrices (filling percentages of the order of 10% or less can lead to a conductivity increasing up to 10 order of magnitudes [91–93]). So strongly superlinear increasing trends with doping are usually attributed to percolation mechanisms. Theoretical results on insulating matrices filled with conducting microstructures, through models based on 2D/3D network description, bond percolation, or statistical/geometrical properties of mixtures [93–95], demonstrate that a slight increase of electrical conductivity should be observed at low doping, and then, increasing the amount of the filling materials, a critical threshold in the doping level is expected (corresponding to the creation a full percolating path), above which the conductivity should exhibit a sudden increase. The specific value of the threshold doping strongly depends on the particular features of both matrix and filling materials. Our results resemble this general qualitative behavior, with the threshold standing around 20% wt. Filling levels much higher than the

threshold should lead to a saturation of the electrical conductivity (corresponding to a complete filling of the available sites in the host matrix), producing a characteristic S-shaped curve of conductivity vs. doping. Our MGL composites did not show saturation up to the highest investigated concentration of GL. However, extrapolating the pure GL as an indication of a hypothetic 100% filled composite, the resulting plot (inset in Fig. 5) seems to indicate a possible saturation occurring at GL content not yet investigated. The relatively large threshold and saturation values for the GL concentration (compared to the ones reported in the mentioned works) suggest a weak interaction between the filler particles inside the matrices, probably due to a good dispersion triggered by the high porosity of the host material [93]. The reduced surface area and pores volume lead, obviously, to a reduced adsorption capacity, as measured in [70]. However, it is worth to note that the increase of 5 order of magnitudes in the dc electrical conductivity from MGL-1 to MGL-4 corresponds to a decrease in the Ar adsorption/desorption isotherms of only 30%; furthermore, the Ar adsorption reduction from HKUST-1 (which, from the electrical point of view is basically insulating) is of a factor 3–4. These remarks prove that the class of composites of Cu-based MOF and GL layers developed in our work, exhibits an enormous increase of dc electrical conductivity with only slight reduction in the porosity and adsorption properties.

In addition to what reported, we would like to mention some preliminary studies that reveal how our GL samples are of potential interest for future technological different applications.
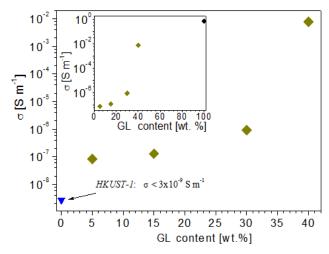
Fig. 5. (color online) electrical conductivity of HKUST-1 (blue), MGL composites (green), and GL (black). (adapted from [70]).

We studied the possibility to realize biocompatible and conductive interfaces for bioelectronics applications by an efficient interfacing of two materials featuring π-π systems, namely the human pigment eumelanin (EU) [96] and GL layers. The hybrid material (EUGL) exhibited adhesion, water stability, biocompatibility towards stem cells and microglia cells [97]. Comparative AFM inspection of the morphologies of EU, GL and EUGL thin films indicates a consistent modification induced by EU to the GL self-assembling. The hybrid film has locally a more granular surface compared to the EU film. EUGL showed strongly improved dc electrical conductivity (more than four orders of magnitude) with respect to the pure pigment due to the presence of embedded GL layers, which could be a key feature in view of biosensing applications. A time-decay of dc electrical conductivity in the eumelanin and hybrid samples was also detected (while this phenomenon is absent in the GL film). On both EU and EUGL samples, such decay seems to be composed by two contributions, exhibiting two different time scales and different quantitative amounts. This double time-scale decay suggests the presence of a double contribution to the electrical transport in both eumelanin and EUGL sample: ionic and electronic. In the GL film the ionic transport (as well a huge trapping of electrons) is missing [97].

Finally, GL layers have been also used to prepare composites with TiO_2 nanoparticles by liquid phase deposition. The photocatalytic activity of the TiO_2/GL composites has been tested for the selective conversion of 3-pyridine methanol to 3-pyridine carboxyaldehyde and nicotinic acid (vitamin B3), under de-aerated and UV/solar simulated conditions, in the presence of cupric ions. Two different composite morphologies have been explored and a dependence of the photocatalytic activity has been assessed, revealing an enhanced photocatalytic activity, with respect to the neat TiO_2, attributed to the broader variety of stable free-radical species generated, at a given photocatalyst morphology, within the delocalized π-electron systems [98]. The antibacterial properties of GL layers also open new possibilities in their exploitation for the fabrication of new biocompatible materials [99].

3. Conclusions

We developed a two-step method for producing graphene-like materials, with some advantages over the conventional method based on graphite oxidation and reduction:

1) graphene-like layers were produced in mild conditions with high yields without the use of hydrazine vapor for the restoring of the graphitic network;

2) all procedures are performed in aqueous environments, which is environmentally advantageous and highly compatible to an industrial scale-up process.

Our approach provides capability for manipulating the physical properties of thin films. In particular, we demonstrated, though combined zeta-potential and AFM measurements, that the quality and the features of the produced self-assembled films are strongly affected by the pH of the water suspension from which the films themselves are prepared. The observed morphologic differences are consistent with the interactions features expected for surfaces having different hydrophilic character as a consequence of a different amount of deprotonation of carboxylic groups: the observation of grains or of flat surfaces can be easily understood in terms of consequent surface tension (macroscopic point of view) or, equivalently, in terms of microscopic interaction between the fundamental units in the water suspension (in particular, related to the carboxylic groups on the film surface).

The graphene-like layers are promising constituents for composite materials. In particular, we explored their incorporation in MOF structures. Thus, we produced and characterized a new class of copper-based-MOF/graphene-like composites, starting from the HKUST-1 metal-organic framework and by varying the graphene-like loading. The main features of HKUST-1 in the composites are preserved, indicating that the interaction of the HKUST-1 units with the carboxylic functionalities of GL does not interfere with the HKUST-1

crystal growing. The incorporation of GL introduces a new porosity in the composites although the surface area of the composites is lower than the HKUST-1, suggesting a distortion in the porous structure of the materials. Preliminary electrical measurements revealed a strong increase of the dc conductivity in the samples as a function of GL content. The tunable conductivity and the new porosity distribution arising by graphene-like incorporation, together with high specific surface area of the composites, can impart new properties to the pristine HKUST-1. The realization of further possible composites with other materials (such as TiO_2 nanoparticles and eumelanin) for different applications (catalysis and biosensing) is also a realistic option.

References

[1]. K.S. Novoselov, A.K. Geim, S.V. Morozov, D. Jiang, Y. Zhang, S.V. Dubonos, I.V. Grigorieva, A.A. Firsov, Science 306 (2004) 666–669.

[2]. M.J. Allen, V.C. Tung, R.B. Kaner, Chem. Rev. 110 (2010) 132–145.

[3]. A.A. Balandin, S. Ghosh, W. Bao, I. Calizo, D. Teweldebrhan, F. Miao, C.N. Lau, Nano Lett. 8 (2008) 902–907.

[4]. K.I. Bolotin, K.J. Sikes, Z. Jiang, M. Klima, G. Fudenberg, J. Hone, P. Kim, H.L. Stormer, Solid State Commun. 146 (2008) 351–355.

[5]. X. Wang, L. Zhi, K. Müllen, Nano Lett. 8 (2008) 323–327.

[6]. K.S. Novoselov, A.K. Geim, S.V. Morozov, D. Jiang, M.I. Katsnelson, I.V. Grigorieva, S.V. Dubonos, A.A. Firvos, Nature 438 (2005) 197–200.

[7]. Y. Zhang, Y.W. Tan, H.L. Stormer, P. Kim, Nature 438 (2005) 201–204.

[8]. C. Lee, X. Wei, J.W. Kysar, J. Hone, Science 321 (2008) 385–388.

[9]. H. Choi, H. Kim, S. Hwang, W. Choi, M. Jeon, Sol. Energy Mater. Sol. Cells 95 (2010) 323–325.

[10]. P. Blake, P.D. Brimicombe, R.R. Nair, T.J. Booth, D. Jiang, F. Schedin, L.A. Ponomarenko, S.V. Morozov, H.F. Gleeson, E.W. Hill, A.K. Geim, K.S. Novoselov, Nano Lett. 8 (2008) 1704–1708.

[11]. M.D. Stoller, S. Park, Y. Zhu, J. An, R.S. Ruoff, Nano Lett. 2008, 8, 3498–3502.

[12]. J.S. Bunch, A.M. van der Zande, S.S. Verbridge, I.W. Frank, D.M. Tanenbaum, J.M. Parpia, H.G. Craighead, P.L. McEuen, Science 315 (2007) 490–493.

[13]. A.K. Geim, K.S. Novoselov, Nat. Mater. 6 (2007) 183–191.

[14]. T. Ramanathan, A.A. Abdala, S. Stankovich, D.A. Dikin, M. Herrera-Alonso, R.D. Piner, D.H. Adamson, H.C. Schniepp, X. Chen, R.S. Ruoff, S.T. Nguyen, I.A. Aksay, R.K. Prud'Homme, L.C. Brinson, Nat. Nanotechnol. 3 (2008) 327–331.

[15]. M. Ruan, Y. Hu, Z. Guo, R. Dong, J. Palmer, J. Hankinson, C. Berger, W.A. de Heer, MRS Bull. 37 (2012) 1138–1147.

[16]. R. Ruoff, Nat. Nanotech. 3 (2008) 10–11.

[17]. O.C. Compton, S.T. Nguyen, Small 6 (2010) 711–723.

[18]. J. Luo, H.D. Jang, T. Sun, L. Xiao, Z. He, A.P. Katsoulidis, M.G. Kanatzidis, J.M. Gibson, J. Huang, ACS Nano 5 (2011) 8943–8949.

[19]. R. Vidic, M. Suidan, G. Sorial, R. Brenner, Water Environ. Res. 65 (1993) 156–161.

[20]. S. Wu, P. Pendleton, J. Colloid Interface Sci. 243 (2001) 306–315.

[21]. S. Kwon, R. Vidic, E. Borguet, Carbon 40 (2002) 2351–2358.

[22]. S. Kwon, R. Vidic, E. Borguet, Surf. Sci. 522 (2003) 17–26.

[23]. C. Li, K. Yao, J. Liang, Carbon 41 (2003) 858–860.

[24]. M. Toebes, F. Prinsloo, J. Bitter, A. van Dillen, K. de Jong, J. Catal. 214 (2003) 78–87.

[25]. N. Beck, S. Meech, P. Norman, L. Pears, Carbon 40 (2002) 531–540.

[26]. Y. Li, C. Lee, B. Gullett, Fuel 82 (2003) 451–457.

[27]. J. Liu, Z. He, S. Wang, New Carbon Mater. 2002 17 (2002) 20–24.

[28]. X. Huang, X. Qi, F. Boeyab, H. Zhang, Chem. Soc. Rev. 41 (2012) 666–686.

[29]. W. Shi, J. Zhu, D.H. Sim, Y.Y. Tay, Z.Y. Lu, X.J. Zhang, H. Zhang, H.H. Hng, Q. Yan, J. Mater. Chem. 21 (2011) 3422–3427.

[30]. J. Zhu, T. Zhu, X. Zhou, Y. Zhang, X.W. Lou, X. Chen, H. Chen, H. Zhang, H.H. Hng, J. Ma, Q. Yan, Nanoscale 3 (2011) 1084–1089.

[31]. X. Huang, S. Li, Y. Huang, S. Wu, X. Zhou, S. Li, C.L. Gan, F. Boey, C.A. Mirkin, H. Zhang, Nat. Commun. 2011, 2, 292_1–6.

[32]. S. Wang, B.M. Goh, K.K. Manga, Q. Bao, P. Yang, K.P. Loh, ACS Nano 4 (2010) 6180–6186.

[33]. T.H. Han, W.J. Lee, D.H. Lee, J.E. Kim, E.Y. Choi, S.O. Kim, Adv. Mater. 22 (2010) 2060–2064.

[34]. H.F. Yang, Q.X. Zhang, C.S. Shan, F.H. Li, D.X. Han, L. Niu, Langmuir 26 (2010) 6708–6712.

[35]. C.H. Lu, H.H. Yang, C.L. Zhu, X. Chen, G.N. Chen, Angew. Chem., Int. Ed. 121 (2009) 4879–4881.

[36]. H. Chang, L. Tang, Y. Wang, J. Jiang, J. Li, Anal. Chem. 82 (2010) 2341–2346.

[37]. Y. Wang, Z. Li, D. Hu, C.-T. Lin, J. Li, Y. Lin, J. Am. Chem. Soc. 132 (2010) 9274–9276.

[38]. X. Dong, B. Li, A. Wei, X. Cao, M.B. Chan-Park, H. Zhang, L.-J. Li, W. Huang, P. Chen, Carbon 49 (2011) 2944–2949.

[39]. V.C. Tung, L.-M. Chen, M.J. Allen, J.K. Wassei, K. Nelson, R.B. Kaner, Y. Yang, Nano Lett. 9 (2009) 1949–1955.

[40]. E. Yoo, J. Kim, E. Hosono, H.-S. Zhou, T. Kudo, I. Honma, Nano Lett. 8 (2008) 2277–2282.

[41]. D. Yu, L. Dai, J. Phys. Chem. Lett. 1 (2009) 467–470.

[42]. Z. Fan, J. Yan, L. Zhi, Q. Zhang, T. Wei, J. Feng,

M. Zhang, W. Qian, F. Wei, Adv. Mater. 22 (2010) 3723–3728.

[43]. M. Jahan, Q. Bao, J.-X. Yang, K.P. Loh, J. Am. Chem. Soc. 132 (2010) 14487–14495.

[44]. C. Petit, T.J. Bandosz, Adv. Funct. Mater. 20 (2010) 111–118.

[45]. C. Petit, J. Burress, T.J. Bandosz, Carbon 49 (2011) 563–572.

[46]. J.H. Lee, D.W. Shin, V.G. Makotchenko, A.S. Nazarov, V.E. Fedorov, Y.H. Kim, J.Y. Choi, J.M. Kim, J.B. Yoo, Adv. Mater. 21 (2009) 4383–4387.

[47]. K.S. Kim, Y. Zhao, H. Jang, S.Y. Lee, J.M. Kim, K.S. Kim, J.H. Ahn, P. Kim, J.H. Choi, B.H. Hong, Nature 457 (2009) 706–710.

[48]. D.S. Li, W. Windl, N.P. Padture, Adv. Mater. 21 (2009) 1243–1246.

[49]. S. Stankovich, D.A. Dikin, R.D. Piner, K.A. Kohlhaas, A. Kleinhammens, Y. Jia, Y. Wu, S.T. Nguyen, R.S. Ruoff, Carbon 45 (2007) 1558–1565.

[50]. L.Y. Jiao, L. Zhang, X.R. Wang, G. Diankov, H.J. Dai Nature 458 (2009) 877–880.

[51]. D. Luo, G. Zhang, J. Liu, X. Sun, J. Phys. Chem. C 115 (2011) 11327–11335.

[52]. H.C. Schniepp, J.L. Li, M.J. McAllister, H. Sai, M. Herrera-Alonso, D.H. Adamson; R.K. Prud'homme, R. Car, D.A. Saville, I.A. Aksay, J. Phys. Chem. B 110 (2006) 8535–8539.

[53]. K.H. Liao, A. Mittal, S. Bose, C. Leighton, K.A. Mkhoyan, C.W. Macosko, ACS Nano 5 (2011) 1253–1258.

[54]. G. Williams, B. Seger, P.V. Kamat, ACS Nano 2 (2008) 1487–1491.

[55]. K. Kinoshita, Carbon-Electrochemical and Physico-chemical Properties; Wiley: New York, 1988.

[56]. J.B. Donnet, R.C. Bansal, M.J. Wang, Carbon Black: Science and Technology, 2nd ed.; Dekker: New York, 1993.

[57]. E. Santini, F. Ravera, M. Ferrari, M. Alfè, A. Ciajolo, L. Liggieri, Colloids Surf. A 365 (2010) 189–198.

[58]. H. Shui, Fuel 84 (2005) 939–941.

[59]. K. Kamegawa, K. Nisiukubo, H. Yoshida, Carbon 36 (1998) 433–441.

[60]. P.G. Ren, D.X. Yan, X. Ji, T. Chen, Z.M. Li, Nanotechnology 22 (2011) 055705.

[61]. I.K. Moon, J. Lee, H. Lee Chem. Commun. 47 (2011) 9681–9683.

[62]. K. Kamegawa, K. Nisiukubo, M. Kodama, Y. Adachi, H. Yoshida Carbon 40 (2002) 1447–1455.

[63]. M. Alfè, V. Gargiulo, R. Di Capua, F. Chiarella, J.N. Rouzaud, A. Vergara, A. Ciajolo, ACS Appl. Mater. Interfaces 4 (2012) 4491–4498.

[64]. Jr.V. Strelko, D.J. Malik, M. Streat Carbon 40 (2002) 95–104.

[65]. H.F. Gorgulho, J.P. Mesquita, F. Goncalves, M.F.R. Pereira, J.L. Figueiredo, Carbon 46 (2008) 1544–1555.

[66]. M. Alfè, V. Gargiulo, R. Di Capua, Appl. Surf. Sci. 353 (2015) 628–635.

[67]. D.H. Everett, Basic Principles of Colloid Science, The Royal Society of Chemistry, London, 1988.

[68]. J.I. Paredes, S. Villar-Rodil, P. Solis-Fernandez, A. Martınez-Alonso, J.M.D. Tascon, Langmuir 25 (2009) 5957–5968.

[69]. P.G. de Gennes, Rev. Mod. Phys. 57 (1985) 827–863.

[70]. M. Alfè, V. Gargiulo, L. Lisi, R. Di Capua, Mater. Chem. Phys. 147 (2014) 744–750.

[71]. N. Stock; S. Biswas, Chem. Rev. 112 (2012) 933–969.

[72]. H. Chae, D. Siberio-Perez, J. Kim, Y. Go, M. Eddaoudi, A. Matzger, M. O'Keeffe, O.M. Yaghi, Nature 427 (2004) 523–527.

[73]. J. Liu, P.K. Thallapally, B.P. McGrail, D.R. Brown Chem. Soc. Rev. 41 (2012) 2308–2322.

[74]. N.A. Khan, Z. Hasan, S.H. Jhung, J. Hazard. Mater. 244−245 (2013) 444–456.

[75]. K. Sumida, D.L. Rogow, J.A. Mason, T.M. McDonald, E.D. Bloch, Z.R. Herm, T.-H. Bae, J.R. Long Chem. Rev. 112 (2012) 724–781.

[76]. J.R. Li, Y. Ma, M.C. McCarthy, J. Sculley, J. Yu, H.K. Jeong, P.B. Balbuena, H.-C. Zhou, Coord. Chem. Rev. 255 (2011) 1791–1823.

[77]. J.R. Li, J. Sculley, H.C. Zhou, Chem. Rev. 112 (2012) 869–932.

[78]. M.P. Suh, H.J. Park, T.K. Prasad, D.W. Lim, Chem. Rev. 112 (2012) 782–835.

[79]. M. Ranocchiari, J.A. van Bokhoven, Phys. Chem. Chem. Phys. 13 (2011) 6388–6396.

[80]. P. Horcajada, R. Gref, T. Baati, P.K. Allan, G. Maurin, P. Couvreur, G. Ferey, R.E. Morris, C. Serre, Chem. Rev. 112 (2012) 1232–1268.

[81]. S. Achmann, G. Hagen, J. Kita, I.M. Malkowsky, C. Kiener, R. Moos, Sensors (2009) 1574–1589.

[82]. S.J. Yang, J.Y. Choi, H.K. Chae, J.H. Cho, K.S. Nahm, C.R. Park, Chem. Mater. 21 (2009) 1893–1897.

[83]. C. Petit, B. Mendoza, D. O'Donnell, T.J. Bandosz, Langmuir 27 (2011) 10234–10242.

[84]. C.H. Hendon, D. Tiana, A. Walsh, Phys. Chem. Chem. Phys. 14 (2012) 13120–13132.

[85]. S.S.Y. Chui, S.M.F. Lo, J.P.H. Charmant, A.G. Orpen, I.D. Williams, Science 283 (1999) 1148–1150.

[86]. C. Prestipino, L. Regli, J.G. Vitillo, F. Bonino, A. Damin, C. Lamberti, Chem. Mater. 18 (2006) 1337–1346.

[87]. J.J. Low, A.I. Benin, P. Jakubczak, J.F. Abrahamian, S.A. Faheem, R.R. Willis, J. Am. Chem. Soc. 131 (2009) 15834–15842.

[88]. A. Santamaria, N. Yang, E. Eddings, F. Mondragon Combust. Flame 157 (2010) 33–42.

[89]. Y.K. Seo, G. Hundal, I.T. Jang, Y.K. Hwang, C.H. Jun, J.S. Chang, Micropor. Mesopor. Mater. 119 (2009) 331–337.

[90]. C. Petit, T.J. Bandosz, Adv. Funct. Mater. 21 (2011) 2108–2117.

[91]. J.C. Huang, C.L. Wu, Adv. Polym. Technol. 19 (2000) 132−139.

[92]. Y. Chekanov, R. Ohnogi, S. Asai, M. Sumita, J. Mater. Sci. 34 (1999) 5589–5592.

[93]. J.-C. Huang Adv. Polym. Technol. 21 (2002) 299–313.

[94]. S. Kirkpatrick, Rev. Mod. Phys. 45 (1973) 574–588.

[95]. F. Lux, J. Mater. Sci. 28 (1993) 285–301.

[96]. M. d'Ischia, K. Wakamatsu, A. Napolitano, S. Briganti, J.C. Garcia-Borron, D. Kovacs, P. Meredith, A. Pezzella, M. Picardo, T. Sarna, J.D. Simon, S. Ito, Pigm. Cell Melanoma Res. 26 (2013) 616–633.

[97]. V. Gargiulo, M. Alfè, R. Di Capua, A.R. Togna, V. Cammisotto, S. Fiorito, A. Musto, A. Navarra, S. Parisi, A. Pezzella, J. Mater. Chem. B 3 (2015) 5070–5079.

[98]. M. Alfè, D. Spasiano, V. Gargiulo, G. Vitiello, R. Di Capua, R. Marotta, Appl. Catal. A-General 487 (2014) 91–99.

[99]. M. Olivi, M. Alfè, V. Gargiulo, F. Valle, F. Mura, M. Di Giosia, S. Rapino, C. Palleschi, D. Uccelletti, S. Fiorito, J. Nanopart. Res. 18 (2016) 358.